JOURNAL OF NATURAL PRODUCTS

Article

Cite This: J. Nat. Prod. XXXX, XXX, XXX−XXX

pubs.acs.org/jnp

Diterpenoids from *Euphorbia dulcis* with Potassium Ion Channel Inhibitory Activity with Selective G Protein-Activated Inwardly Rectifying Ion Channel (GIRK) Blocking Effect

Norbert Kúsz,[†] Péter Orvos,[‡,§] Laura Bereczki,[⊥] Pierre Fertey,[∥] Petra Bombicz,[⊥] Attila Csorba,[†] László Tálosi,[§] Gusztáv Jakab,[▽] Judit Hohmann,*[,†,#] and Dóra Rédei[†]

[†]Department of Pharmacognosy, [‡]Department of Pharmacology and Pharmacotherapy, and [#]Interdisciplinary Centre for Natural Products, Interdisciplinary Excellence Centre, University of Szeged, 6720 Szeged, Hungary

[§]Rytmion Ltd., 6724 Szeged, Hungary

[⊥]Research Centre for Natural Sciences, Hungarian Academy of Sciences, 1117 Budapest, Hungary

[∥]Synchrotron SOLEIL L'Orme des Merisiers−Saint Aubin, B.P. 4891 192 Gif-sur-Yvette Cedex, France

[▽]Institute of Environmental Sciences, Faculty of Water and Environmental Management, Szent István University, 5540 Szarvas, Hungary

Supporting Information

ABSTRACT: Nine new (**1**−**9**) and two known (**10**, **11**) jatrophane diterpenoids were isolated from the methanol extract of *Euphorbia dulcis*. The structure elucidation of the compounds was performed by means of extensive spectroscopic analysis, including HRESIMS, 1D (^{1}H, JMOD), and 2D (HSQC, HMBC, ^{1}H−^{1}H-COSY, NOESY) NMR experiments. The absolute configuration of compound **1** was determined by single-crystal X-ray diffraction. The electrophysiological effects of compounds **1**−**11** and the five diterpenoids (**12**−**16**) previously isolated from *Euphorbia taurinensis* were investigated on stable transfected HEK-GIRK1/4 (Kir3.1/3.4) and HEK-hERG (Kv11.1) cell lines using automated patch-clamp equipment. The majority of the diterpenoids showed significant blocking activity on GIRK channels (60.8−88.7% at 10 μM), while compounds **1**, **2**, **9**−**11**, **13**, and **14** exerted notable inhibitory effects even at 1 μM concentration. None of the jatrophane diterpenoids interfered with the function of hERG proteins; however, compound **14** remarkably hampered K^+ flow through hERG channels. These selective activities suggest that jatrophane diterpenoids may represent a group of potential lead compounds for the development of novel therapeutic agents against atrial fibrillation.

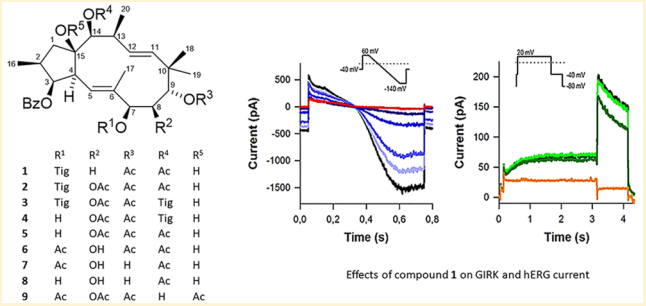

	R1	R2	R3	R4	R5
1	Tig	H	Ac	Ac	H
2	Tig	OAc	Ac	Ac	H
3	Tig	OAc	Ac	Tig	H
4	H	OAc	Ac	Tig	H
5	H	OAc	Ac	Ac	H
6	Ac	OH	Ac	Ac	H
7	Ac	OH	H	Ac	H
8	H	OH	H	Ac	H
9	Ac	OAc	Ac	H	Ac

Atrial fibrillation (AF) is the most common form of sustained cardiac arrhythmia in adults. It is characterized by uncoordinated supraventricular activation and consequently ineffective, quivering, or irregular atrial contractions.[1] As a prominent risk factor of life-threatening cardiovascular conditions such as thrombo-embolism, stroke, and heart failure, AF accounts for huge and rapidly growing healthcare expenditures in Western countries.[2,3] Despite the continuous improvement of therapeutic strategies, AF still contributes to an estimated 130 000 deaths each year just in the U.S.[4] Current antiarrhythmic drugs (AADs) have numerous disadvantages, most importantly the lack of atrial specificity associated with an increased risk of side effects and the poor efficacy rate (e.g., 50−60% for amiodarone, which is generally considered as the most effective AAD).[5] This background underlines the constant need for the development of more targeted AADs.

Although the pathomechanism of AF is not yet fully understood, it has been described that elevated vagal nerve tone can induce ion-channel-mediated detrimental electrophysiological alterations in the atrial muscle tissue.[6] Ion channels are pore-forming transmembrane proteins that are classified into ligand-gated and voltage-gated groups. GIRK channels (G protein-activated inwardly rectifying potassium channels) are activated by acetylcholine and are involved in the fine electrical regulation of neurons, β-pancreatic cells, and atrial myocytes. Malfunctions of GIRK proteins are suspected to contribute to the development of neuropathic pain, drug addiction, and cardiac arrhythmias.[7] This hypothesis is supported by recent animal studies in which tertiapin, a peptide isolated from bee venom, terminated AF episodes by prolonging the atrial effective refractory period through selective blockade of GIRK channels.[8]

Received: July 3, 2018

DOI: 10.1021/acs.jnatprod.8b00500
J. Nat. Prod. XXXX, XXX, XXX−XXX

hERG channels (human ether-a-go-go-related gene encoded potassium channels) are members of the K^+-permeable voltage-gated membrane proteins ("K_v channel class") frequently referred to as Kv11.1. hERG channels pass the rapid component of delayed rectifier K^+ current (I_{Kr}) and thus influences the duration of the plateau phase and the pacemaking activity of sinoatrial and atriventricular node cells.[9] A wide range of structurally unrelated drugs such as psychiatric, antimicrobial, antihistamine, and even antiarrhythmic agents have been shown to possess strong affinity toward hERG channels.[10,11] The consequent drug-induced QT interval prolongation in the EKG predisposes patients to Torsades de Pointes (TdP) arrhythmias and sudden cardiac death. Several drugs have been withdrawn from the market because of fatalities caused by prolonged QT and subsequent TdP.[12] Given the clinical importance of the proarrhythmogenic potential of commonly used pharmaceuticals, screening drug candidates for their hERG channel selectivity during preclinical safety assessments is a common practice nowadays.

Natural products represent a vast source of compounds with astonishing chemical and pharmacological diversity. Diterpenoids are characteristic secondary metabolites of Euphorbiaceae species with well-established multidrug-resistance-reversing,[13] antiproliferative,[14] and antiviral properties.[15] However, a limited amount of data are available on their cardiac effects. Diterpenoids with myrsinane, premyrsinane, and cyclomyrsinane skeletons isolated from *Euphorbia falcata* were described as selective blockers of GIRK proteins,[16] while daphnane-type orthoesters of the active fraction of *Gnidia polycephala* exerted hERG channel inhibitory activity.[17] Our research group reported for the first time that jatrophane-type diterpenoids from *Euphorbia guyoniana* are able to substantially prevent K^+ flow ($I_{K,Ach}$) through GIRK channels.[18]

Euphorbia dulcis L. is a perennial plant distributed in West and Central Europe. Its chemical constituents have been barely investigated; only four flavonol glycosides were isolated from the methanol extract of the plant.[19] As part of the ongoing phytochemical examination of Euphorbiaceae species, we describe the isolation and structure determination of nine new (**1**–**9**) and two known [euphomelliferene B (**10**), euphornin (**11**); structures in the Supporting Information] jatrophane diterpenoids. The GIRK channel inhibitory activities of the isolated compounds and five additional diterpenoids obtained from the methanol extract of *E. taurinensis*,[20] namely, 5-acetoxy-3,9-dicinnamoyloxy-15-hydroxy-14-oxojatropha-6(17),11*E*-diene (**12**), 3-*O*-angeloyl-20-deoxyingenol (**13**), 3-*O*-angeloyl-17-angeloyloxy-20-deoxyingenol (**14**), 20-*O*-acetyl-3-*O*-angeloyl-17-angeloyloxyingenol (**15**), and 6,14-diacetoxy-5-(2-acetoxyacetoxy)-3-benzoyloxy-15-hydroxy-9-oxosegetane (**16**), were investigated on the stable transfected HEK-GIRK1/4 (Kir3.1/3.4) cell line. The most potent blockers of GIRK proteins were further tested for their hERG-related cardiotoxicity on HEK-hERG (Kv11.1) cells.

RESULTS AND DISCUSSION

Characterization of Compounds 1–11. Compound **1** was isolated as white, amorphous granules. The peak of the protonated molecule displayed at *m/z* 625.3371 (calcd 625.3377) in the HRESIMS data suggested the molecular formula $C_{36}H_{48}O_9$. The ^1H and JMOD spectra showed distinctive signals of a benzoyl (δ_H 7.98 d, 7.49 t, 7.38 t; δ_C 165.8, 132.8, 130.4, 130.0, and 128.5), two acetyl (δ_H 2.19 s, 1,86 s; δ_C 171.4, 169.5, 2 × 21.2), and a tigloyl (δ_H 6,50 q, 1.28 d, 1.23 s; δ_C 166.6, 137.8, 128.1, 14.3, and 11.4) group (Tables 1 and 2). In combination with the ^1H and ^{13}C NMR data, the molecular formula indicated that **1** is a bicyclic diterpenoid with a disubstituted (δ_H 5.65 dd, 5.11 d; δ_C 138.3, 129.6) and a trisubstituted (δ_H 5.69 d; δ_C 135.1, 119.8) olefinic bond satisfying the 13 indices of hydrogen deficiency. Interpretation of HSQC cross-peaks allowed the assignment of the polyester core comprising five methyls, two methylenes, seven methines (including four oxymethines), and three olefinic carbons. Resonances at δ_C 135.1, 84.0, and 40.2 that did not exhibit any correlations were classified as a nonprotonated sp^2, an oxygenated tertiary, and a quaternary carbon, respectively. Apart from the benzoyl and tigloyl groups, three sequences of correlated protons were identified from the ^1H–^1H-COSY spectrum: $-CH_2-CH(CH_3)-CH(OR)-CH-CH=$ (δ_H 2.04 m, 1.74 m, 2.11 m, 0.90 d, 5.38 br s, 2.89 dd, 5.69 d) [A]; $-CH(OR)-CH_2-CH(OR)-$ (δ_H 5.08 br s, 1.99 m, 4.86 br s) [B]; and $-CH=CH-CH(CH_3)-CH(OR)-$ (δ_H 5.11 d, 5.65 dd, 2.56 m, 0.94 d, 4.91 d) [C] (Figure 1). Additionally, a weak $^4J_{H,H}$ (*W*-type) interaction between the protons resonating at δ_H 5.69 and 1.75 implied their close proximity in the diterpenoid scaffold. The connectivities of COSY spin systems were established by an HMBC experiment. $^2J_{C,H}$ and $^3J_{C,H}$ couplings of H-1α, H-1β, H-3, H-4, and C-15, together with H-14/C-1, revealed the presence of a cyclopentane moiety and the linkage of subunits A and C through C-15. Long-range correlations between H-9, H-12, H_3-18, H_3-19, and C-10 demonstrated that structural fragments B and C and two geminal methyls are involved in the formation of a 12-membered macrocycle characteristic of the jatrophane diterpenoid core. The lack of exomethylene signals and strong cross-peaks of the deshielded H_3-17 with C-5, C-6, and C-7 unambiguously proved that compound **1** contains a rare $\Delta^{5(6)}$ olefinic bond instead of the regular $\Delta^{6(17)}$ double bond. The locations of the ester functionalities were determined via $^3J_{C,H}$ interactions of skeletal oxymethine protons H-3, H-7, H-9, and H-14 with carbonyl carbons at δ_C 165.8 (benzoyl), 166.6 (tigloyl), 169.5, and 171.4 (acetyls), respectively. The relative configuration was defined by analyzing the NOESY spectrum and the pattern of coupling constants. NOE correlations of the reference H-4α with H-2, H-3, H-13, and H-14 confirmed the

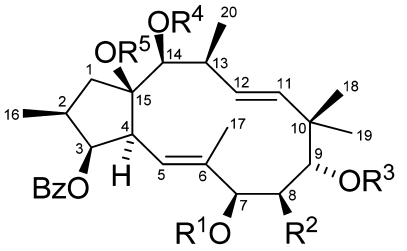

	R^1	R^2	R^3	R^4	R^5
1	Tig	H	Ac	Ac	H
2	Tig	OAc	Ac	Ac	H
3	Tig	OAc	Ac	Tig	H
4	H	OAc	Ac	Tig	H
5	H	OAc	Ac	Ac	H
6	Ac	OH	Ac	Ac	H
7	Ac	OH	H	Ac	H
8	H	OH	H	Ac	H
9	Ac	OAc	Ac	H	Ac
10	Ac	OAc	Ac	Ac	H
11	Ac	H	Ac	Ac	H

DOI: 10.1021/acs.jnatprod.8b00500
J. Nat. Prod. XXXX, XXX, XXX–XXX

Table 1. ^{1}H NMR Data of Compounds 1−9 at 500 MHz (δ_H in ppm, J in Hz)

position	1[a]	2[b]	3[b]	4[a]	5[a]	6[c]	7[a]	8[a]	9[a]
1α	2.04, m	2.10, dd (12.9, 7.1)	2.12, dd (12.9, 7.2)	2.06, m	2.03, dd (13.2, 6.7)	2.52, dd (12.3, 6.5)	2.06, dd (13.0, 6.5)	2.08, dd (12.6, 6.6)	2.95, br d (7.0)
1β	1.74, m	1.72, t (12.9)	1.70, t (12.9)	1.70, t (12.9)	1.74, t (12.9)	2.19, t (12.3)	1.75, t (13.0)	1.73, m	2.14, m[o]
2	2.11, m	2.12, m	2.20, m	2.14, m	2.16, m	2.27, m	2.13, m	2.14, m	2.14, m[o]
3	5.38, br s	5.35, br t (3.6)	5.36, br t (3.6)	5.39, br t (4.2)	5.41, br t (4.3)	5.79, br s	5.42, br s	5.38, br s	5.41, dd (3.9, 2.5)
4	2.89, dd (10.4, 4.8)	3.11, dd (10.0, 4.5)	3.11, dd (10.0, 4.6)	2.97, dd (10.5, 5.1)	2.98, dd (10.5, 5.1)	3.22, dd (9.8, 4.7)	2.84, dd (9.8, 4.5)	2.88, dd (10.0, 4.6)	2.99, dd (9.8, 3.9)
5	5.69, d (10.4)	5.85, br d (9.3)	5.87, br d (8.9)	5.94, d (10.5)	5.94, d (10.5)	6.33, d (9.8)	5.63, br d (8.8)	5.66, d (10.0)	5.75, d (9.8)
7	5.08, br s	5.08, br s	5.10, br s	3.99, d (3.4)	4.01, br d (3.2)	5.51, br s	5.04, br s	4.15, br s	4.96, br s
8	1.99, m (2H)	5.14, br s	5.16, br s	5.15, d (4.0)	5.17, d (4.4)	4.28, d (8.2)	3.71, br s	3.58, br s	5.07, br s[o]
9	4.86, br s	5.31, br s	5.32, br s	4.54, d (3.8)	4.53, d (4.2)	5.63, br s	3.33, br d (5.5)	3.36, br s	5.07, br s[o]
11	5.11, d (15.8)	5.10, d (15.7)	5.13, d (15.7)	5.12, d (15.7)	5.11, d (15.6)	5.34, d (15.8)	5.04, d (15.4)	5.06, d (15.7)	5.09, d (15.7)
12	5.65, dd (15.8, 9.0)	5.97, dd (15.7, 8.5)	5.99, dd (15.7, 8.5)	5.65, dd (15.7, 9.2)	5.65, dd (15.6, 9.3)	6.38, dd (15.8, 8.4)	5.63, dd (15.4, 8.8)	5.61, dd (15.7, 8.9)	5.57, dd (15.7, 8.6)
13	2.56, m	2.68, m	2.71, m	2.62, m	2.62, dq (6.9, 9.3)	2.85, m	2.49, m	2.51, m	2.41, m
14	4.91, d (2.2)	4.95, d (2.6)	5.01, d (2.5)	4.97, d (2.5)	4.94, d (2.8)	5.31, br s	4.92, br s	4.90, br s	3.54, t (2.6)
16	0.90, d (6.4)	0.88, d (6.6)	0.88, d (6.6)	0.95, d (6.7)	0.98, d (6.7)	1.01, d (6.4)	0.96, d (6.6)	0.96, br d (6.1)	0.99, d (5.7)
17	1.75, s	1.89, s	1.90, s	1.78, s	1.80, s	1.92, s	1.80, s	1.74, s	1.87, s
18	0.93, s	0.98, s	0.99, s	1.03, s	1.05, s	1.22, s	1.12, s	1.09, s	0.93, s
19	0.87, s	0.86, s	0.87, s	0.91, s	0.93, s	1.29, s	0.83, s	0.86, s	0.85, s
20	0.94, d (7.5)	0.95, d (7.0)	0.93, d (6.9)	0.93, d (7.0)	0.95, d (6.9)	1.17, d (6.5)	0.96, d (6.6)	0.96, br d (6.1)	1.14, d (7.0)
OBz-3	7.98, d (7.4)	7.99, d (7.4)	7.99, d (7.4)	8.03, d (7.4)	8.05, d (7.4)	8.26, d (7.8)	8.04, d (7.8)	8.02, d (7.5)	7.99, d (7.4)
	7.38, t (7.6)	7.44, t (7.7)	7.44, t (7.8)	7.40, t (7.8)	7.43, t (7.8)	7.25, t (7.5)	7.43, t (7.5)	7.43, t (7.3)	7.45, t (7.6)
	7.49, t (7.2)	7.58, t (7.4)	7.57, t (7.5)	7.50, t (7.4)	7.52, t (7.4)	7.42, t (7,2)	7.53, t (7.3)	7.54, t (7.3)	7.56, t (7.4)
R^1-7	−OTig	−OTig	−OTig	−OH	−OH	−OAc	−OAc	−OH	−OAc
	6.50, q (6.6)	6.57, q (6.3)	6.57, q (6.8)	3.78, br s	3.90, br s	1.32, s	1.25, s	n.o.	1.12, s
	1.28, d (6.8)	1.31, br d (5.7)	1.30, br d (5.7)						
	1.23, s	1.24, s	1.25, s						
R^2-8		−OAc	−OAc	−OAc	−OAc	−OH	−OH	−OH	−OAc
		2.04, br s	2.04, br s	2.03, s	2.05, s	5.70, d (8.2)	4.12, br s	n.o.	2.04, s
R^3-9	−OAc	−OAc	−OAc	−OAc	−OAc	−OAc	−OH	−OH	−OAc
	1.86, s	1.99, s	1.99, s	2.09, s	2.10, s	2.13, s	2.70, d (7.2)	n.o.	2.06, s
R^4-14	−OAc	−OAc	−OTig	−OTig	−OAc	−OAc	−OAc	−OAc	−OH
	2.19, s	2.20, s	7.07, dq (6.9, 0.9)	6.96, dq (6.9, 1.1)	2.26, s	2.12, s	2.23, s	2.23, s	4.93, d (2.6)
			1.87, d (6.9)	1.83, d (6.9)					
			1.92, br s	1.89, br s					
R^5-15	−OH	−OH	−OH	−OH	−OH	−OH	−OH	−OH	−OAc
	n.o.	n.o.	n.o.	n.o.	n.o.	n.o.	n.o.	n.o.	2.41, s

[a]Measured in $CDCl_3$. [b]Measured in methanol-d_4. [c]Measured in pyridine-d_5. [o]Overlapping signals; n.o.: not observed.

β-orientation of the secondary methyls H_3-16 and H_3-20, the C-3 benzoyl group, and the C-14 acetyl group. The C-1 geminal proton pair were readily distinguished via the H-1α/H-14 and H-1β/H_3-16 interactions. The large coupling constant between H-4 and H-5 ($^3J_{H4,5}$ = 10.4 Hz) confirmed their location on the opposite sides of the molecule.[21] With regard to diagnostic NOE-enhanced signals of H-4/H_3-17 and H-5/H-9, as well as the absence of a H-5/H_3-17 correlation, the trisubstituted $\Delta^{5(6)}$ olefinic bond must have an *E*-configuration.[22] Important cross-peaks of H-7/H_3-17 and H-9/H_3-18 clearly dictated the β-position of the tigloyl and the α-orientation of the acetyl groups located at C-7 and C-9, respectively. Furthermore, the *E*-configuration of the $\Delta^{11(12)}$ double bond was evident from the large $^3J_{H11,12}$ value (15.8 Hz). The 12-membered macrocycles are known to be quite flexible; however, concerning the sharp proton signals it is most likely that molecules were undergoing fast interconversions between two or more conformations in solution. Considering the large value of $^3J_{H4,5}$ and the restricted rotation around the C-5/C-6 axis, it was clear that the H_3-17 methyl is predominantly orthogonal to the mean plane of the macrocycle, implying that compound **1** preferentially adopted an *endo*-type conformation.[21,23]

The absolute configuration of compound **1** was determined by single-crystal X-ray diffraction. Single crystals of size around 0.05 × 0.1 × 2−3 mm were grown from a mixture of acetonitrile and water. The saturated solution was seeded by minuscule crystals obtained from the melt of the compound

DOI: 10.1021/acs.jnatprod.8b00500
J. Nat. Prod. XXXX, XXX, XXX−XXX

Table 2. ^{13}C NMR Data of Compounds 1−9 at 125 MHz (δ_C in ppm)

position	1[a]	2[b]	3[b]	4[a]	5[a]	6[c]	7[a]	8[a]	9[a]
1	46.2	48.8	48.5	46.4	46.3	48.4	46.9	46.6	44.9
2	37.4	38.3	38.4	36.9	37.0	37.4	36.9	37.1	37.9
3	81.0	82.9	82.9	81.3	81.2	82.0	81.1	81.5	79.9
4	48.1	48.7	48.8	48.0	48.0	48.5	47.9	48.1	48.6
5	119.8	124.3	124.4	121.9	122.0	122.8	122.1	120.2	121.1
6	135.1	132.2	132.4	134.8	134.9	131.6	130.7	136.2	131.3
7	73.5	79.5	79.6	77.5	77.5	82.8	81.8	79.9	77.5
8	32.5	69.6	69.6	69.6	69.5	68.3	68.0	68.0	68.0
9	73.9	73.7	73.7	73.5	73.8	74.3	72.4	71.8	72.2
10	40.2	41.0	41.1	39.3	39.5	40.2	40.1	39.8	39.3
11	138.3	135.9	136.1	136.8	136.9	135.6	139.5	139.6	135.5
12	129.6	134.1	134.2	130.3	130.4	133.0	128.8	128.8[e]	130.5
13	39.5	40.0	40.4	39.7	39.9	39.5	39.7	39.4	39.8
14	81.2	82.6	82.6	81.0	81.1	81.6	80.9	81.0	81.1
15	84.0	84.3	84.6	84.4	84.5	83.8	84.1	84.3	94.8
16	13.9	14.2	14.2	13.9	13.9	14.3	13.6	13.9	13.3
17	16.7	16.6	16.6	16.1	16.2	16.8	16.6	16.7	15.8
18	22.9	23.5	23.4	22.8	22.8	23.5	22.9	23.1	22.0
19	20.5	21.3	21.3	21.0	21.0	21.7	19.0	19.2	19.4
20	19.4	20.2	20.0	19.3	19.4	20.4	19.9	19.5	20.4
BzO-3	165.8	167.3	167.4	166.5	166.7	166.1	165.6	166.4	164.9
	130.4	131.6	131.6	130.6	130.8	131.4	130.3	130.2	129.9
	130.0	131.0	131.0	130.0	129.9	130.6	129.9	129.9	129.5
	128.5	129.7	129.7	128.6	128.6	129.0	128.7	128.8[e]	128.5
	132.8	134.2	134.2	133.0	133.0	133.3	133.2	133.3	133.1
TigO-7	166.6	168.2	168.2						
	128.1	128.7	128.7						
	137.8	139.7	139.8						
	14.3	14.5	14.5						
	11.4	12.0	12.0						
AcO-7						170.0	172.5		168.9
						20.3	19.8		20.1
AcO-8		172.0	172.1	169.7	169.9				170.2
		21.0[e]	21.1[e]	21.2	21.2				21.0
AcO-9	169.5	171.6	171.6	172.1	172.2	169.6			169.2
	21.2[e]	21.0[e]	21.1[e]	20.9	20.9	21.2[e]			20.8
AcO-14	171.4	173.3			171.2	171.8	171.3	171.3	
	21.2[e]	21.1			21.3	21.2[e]	21.2	21.2	
TigO-14			170.0	168.2					
			129.8	128.4					
			139.6	138.4					
			14.7	14.9					
			12.5	12.1					
AcO-15									174.3
									22.0

[a]Measured in $CDCl_3$. [b]Measured in methanol-d_4. [c]Measured in pyridine-d_5. [e]Exchangeable signals.

(see details in the Supporting Information). When a traditional sealed tube X-ray source is used, reflections of the transparent, needle-like crystals were weak. A higher intensity beam was necessary in order to measure high-angle reflections; therefore data collection was performed on a single crystal of **1** (size 0.02 × 0.02 × 0.15 mm) at the synchrotron source SOLEIL, on the PROXIMA 1 beamline (λ = 0.799 90 Å, beam size HxV = 40 × 30 μm^2) at −173 °C in the θ-range of 1.682−31.198°. Details of crystal and structural data can be found in the Supporting Information.

Compound **1** crystallizes in the monoclinic chiral space group $P2_1$ with three crystallographically independent but chemically identical molecules in the asymmetric unit. The absolute configuration has been established in the diffraction measurement based on the anomalous dispersion effect of the nine oxygen atoms present in the molecule. For all three conformers of **1**, the assignment is most likely (2*S*,3*S*,4*S*,7*R*,9*R*,13*S*,14*S*,15*R*)-9α,14β-diacetoxy-3β-benzoyloxy-15β-hydroxy-7β-tigloyloxyjatropha-5*E*,11*E*-diene (Figure 2). Thus, all three crystallographically independent molecules in the asymmetric unit have the same configuration (Figure 3).

The cyclopentane rings constructed by C-1, C-2, C-3, C-4, and C-15 are in an envelope form with C-2 extending above the plane by the closest puckering descriptors in rings indicated by C-1 and C-1″, while twisted on C-2′−C-3′ in the ring indicated by C-1′ (the three chemically identical but

DOI: 10.1021/acs.jnatprod.8b00500
J. Nat. Prod. XXXX, XXX, XXX−XXX

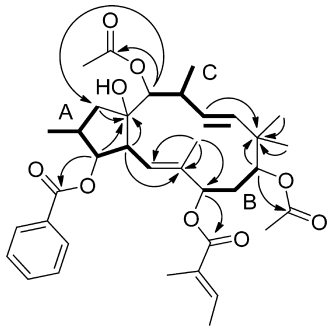

Figure 1. Key 2D NMR correlations for **1**. Bold bonds indicate COSY; arrows indicate HMBC (H → C) correlations.

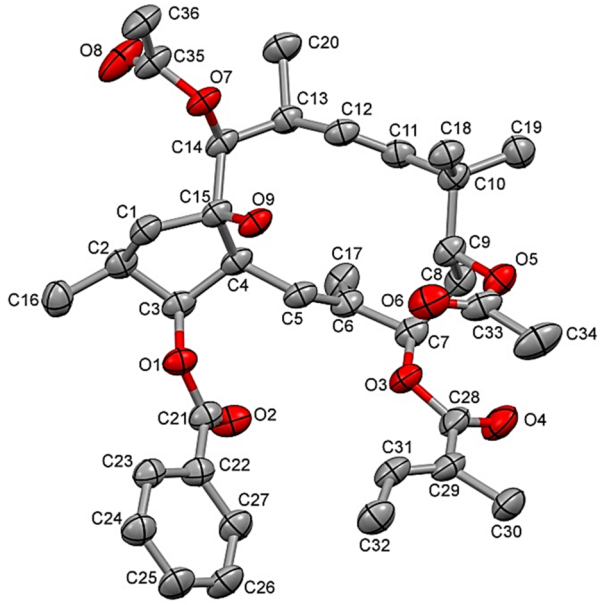

Figure 2. Molecular structure of compound **1** with atomic labeling. The displacement ellipsoids are drawn at the 50% probability level.

crystallographically independent molecules ($Z' = 3$) are labeled without a prime, with one prime, and with two primes, respectively). The angles of the five-membered ring and the aromatic ring in the independent molecules are 69.9(2)°, 82.0(3)°, and 64.5(2)°, respectively. The conformational differences of the core of the molecules are not large in spite of the potential flexibility of the 12-membered macrocycle. Superimposing the core ring systems of the three molecules fits well (Figure 3A), and the atomic positions in the terminal part of the substituents differ (Figure 3B).

Compound **2** was obtained as a white, amorphous solid. Its HRESIMS spectrum exhibited a sodium adduct ion at m/z 705.3281 $[M + Na]^+$ (calcd 705.3251), indicating the molecular formula $C_{38}H_{50}O_{11}$. Comparison of the spectroscopic data of **1** and **2** showed that the structures differed only in an acetoxy group (Tables 1 and 2). This conclusion was substantiated by the presence of an sp^3 oxymethine and methyl resonances at δ_H 5.14 and δ_H 2.04, which gave HMBC correlations with a carbonyl carbon at δ_C 172.0. Further long-range couplings of H-7/C-8, H-8/C-9, and H-8/C-10 suggested that the acetoxy moiety is attached to C-8. Moreover, the zero or small coupling constants $^3J_{H7,8}$ and $^3J_{H8,9}$ are characteristic features of the 7,8,9-trisubstituted jatrophane derivatives.[22,23] The β-orientation of 8-OAc was proven by NOE cross-peaks of H-8 with H_3-17 and H_3-19, while the other eight stereogenic centers were found to be identical with those of compound **1**.

Compound **3** was obtained as a white, amorphous powder. Its molecular formula was deduced to be $C_{41}H_{54}O_{11}$ from the HRESIMS sodium adduct ion at m/z 745.3596 $[M + Na]^+$ (calcd 745.3564). Comprehensive analysis of ^1H, JMOD, and 2D data indicated the presence of the same parent system and esterification pattern as in compound **2**, with the exception of C-14, on which the acetyl group was replaced by an tigloyloxy moiety (Tables 1 and 2). Proton signals of 7-OTig (δ_H 6.57 q, 1.30 br d, 1.25 s) were significantly shielded compared to those of 14-OTig (7.07 dq, 1.92 br s, 1.87 d), which was caused by the anisotropic effect of the *cis*-located C-3 aromatic substituent.[24] The relative configurations of stereogenic carbons were determined by means of a NOESY experiment.

Compound **4** was isolated as white granules, and its formula was assigned as $C_{36}H_{48}O_{10}$ in accordance with the HRESIMS sodium adduct ion at m/z 663.3172 $[M + Na]^+$ (calcd 663.3145). The lack of diamagnetic shifted signals attributed to 7-OTig and an additional hydrogen resonance at δ_H 3.78 with no HSQC cross-peak demonstrated that the difference between **4** and **3** involved the absence of the acyl residue at

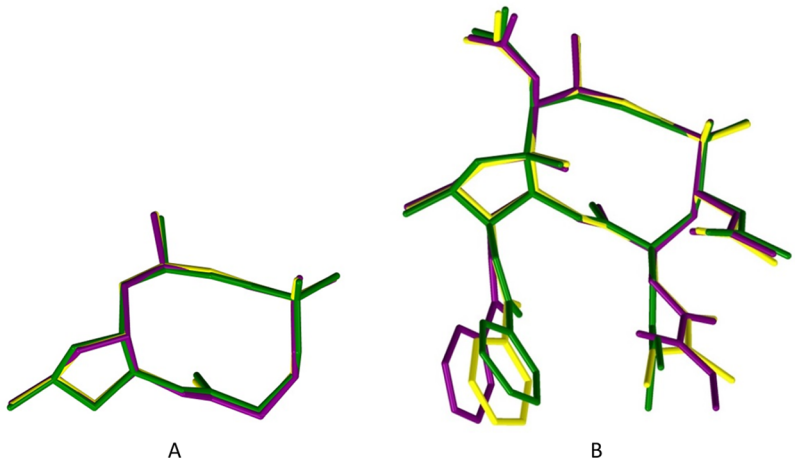

Figure 3. Panel A shows the unit cell of **1**. Panel B represents the molecular overlay of the three crystallographically independent conformers of **1**. [The molecules in the asymmetric unit are distinguished by colors: yellow (C1), green (C1′), and purple (C1″).]

DOI: 10.1021/acs.jnatprod.8b00500
J. Nat. Prod. XXXX, XXX, XXX−XXX

C-7 (Tables 1 and 2). NOE interactions of this hydroxy proton with H-9, as well as H-7/H-8 and H-7/H_3-17, permitted assignment of the same configuration as in **3**.

Compound **5**, $C_{33}H_{44}O_{10}$, was shown to be the 14-*O*-acetyl analogue of **4** by the sodium adduct HRESIMS ion at *m/z* 623.2858 $[M + Na]^+$ (calcd 623.2832) and its 2D NMR spectra. Heteronuclear $^2J_{C,H}$ and $^3J_{C,H}$ correlations of acyl methyls (δ_H 2.05 s, 2.10 s, 2.26 s) and skeletal oxymethines (δ_H 5.17 d, 4.53 d, 4.94 d) with ester carbonyls (δ_C 169.9, 172.2, 171.2) (Tables 1 and 2) provided key information regarding the exact location of substituents. Similar considerations led to the determination of compound **6** as an isomer of **5**, possessing the hydroxy group at C-8 instead of C-7 (Tables 1 and 2).

Compound **7**, $C_{31}H_{42}O_9$, could be derived from **6** by the loss of an acetyl unit compatible with the sodiated HRESIMS ion at *m/z* 581.2732 $[M + Na]^+$ (calcd 581.2766). Evaluation of the HMBC spectrum in conjunction with mutual $^1H-^1H$-COSY couplings of vicinal hydroxy groups (δ_H 4.12 br s, 2.70 d) with neighboring H-8 and H-9 methines (δ_H 3.71 br s, 3.33 br d) established the final structure bearing acetoxy groups at C-7 and C-14 (Tables 1 and 2). The spatial orientation of 7-OAc in the shielding cone of the C-3 *cis*-benzoyl group was apparent from its diamagnetic shifted protons compared to 14-OAc hydrogens (1.25 and 2.23 s, respectively). The molecular formula of **8** was assigned as $C_{29}H_{40}O_8$ using the sodium adduct ion $[M + Na]^+$ observed at *m/z* 539.2644 $[M + Na]^+$ (calcd 539.2621). ^1H and JMOD NMR spectra showed corresponding signals for only one acetoxy group that, based on HMBC cross-peaks of H-14 (δ_H 4.90 br s) and the ester methyl (δ_H 2.23 s) with a carbonyl carbon at δ_C 171.3 (Tables 1 and 2), must be attached to C-14.

Compound **9** has the molecular formula $C_{35}H_{46}O_{11}$, determined by the HRESIMS sodium adduct ion at *m/z* 665.2960 $[M + Na]^+$ (calcd 665.2938). The major differences between **9** and jatrophanes **1**−**8** were the remarkable paramagnetic shifts of the C-1 geminal protons (δ_H 2.95 br d, 2.14 m), the acetyl resonance at δ_H 2.41, and the oxygenated tertiary C-15 at δ_C 94.8 (Tables 1 and 2). In order to define the structure, a complete series of 2D NMR spectra were recorded and analyzed. Compound **9** is a structural isomer of the known euphomelliferene B,[22] in which the ester and hydroxy substituents at C-14 and C-15 were interchanged. This unusual feature was confirmed by the COSY correlation between H-14 (δ_H 3.54 t) and a hydroxy signal (δ_H 4.93 d) and by the absence of HMBC cross-peaks of the acetyl carbonyl carbon (δ_C 174.3) with skeletal protons. A set of NOE effects revealed the same relative configuration of the stereogenic carbons. Given the fact that all of the jatrophane diterpenoids isolated to date contain a *trans*-fused cyclopentane ring, the 15-OAc moiety is assumed to occupy a *β*-position.[25]

According to the literature data, compounds **10** and **11** were identified as euphomelliferene B and euphornin, respectively.[22,26]

Effects of Compounds on GIRK and hERG Potassium Channels. In order to find effective natural agents for the treatment of atrial fibrillation, screening of the diterpenoids with different skeletons and substitution patterns isolated from *E. dulcis* (**1**−**11**) and *E. taurinensis* (**12**−**16**) was performed on the GIRK channel expressing cell line. Compounds were screened in two concentrations (1 and 10 μM) on two or three cells. The majority of the diterpenoids possessed significant blocking activity at 10 μM concentration on the GIRK channel, and some of these compounds exhibited notable inhibitory effects even at a 1 μM concentration (Table 3).

Table 3. Electrophysiological Effects of Compounds 1−16 on GIRK Current in HEK-GIRK Cells[a]

	GIRK inhibition (%)		
	concentration		propafenone
compound	1 μM	10 μM	1 μM
1	35.5 ± 5.6	88.7 ± 2.4	93.2 ± 1.7
2	38.5 ± 3.5	85.0 ± 0.8	92.6 ± 3.2
3	23.5 ± 0.3	35.7 ± 7.4	70.1 ± 5.9
4	15.3 ± 2.7	60.8 ± 6.8	60.6 ± 2.6
5	16.8 ± 2.1	66.6 ± 3.5	64.2 ± 2.5
6	16.0 ± 10.2	26.8 ± 6.9	65.2 ± 3.4
7	11.2 ± 6.3	23.5 ± 3.3	72.7 ± 1.5
8	15.7 ± 9.0	25.7 ± 1.7	69.4 ± 3.0
9	27.2 ± 4.8	66.0 ± 8.2	76.3 ± 6.7
10	33.8 ± 4.9	83.4 ± 0.6	94.2 ± 2.4
11	31.1 ± 1.9	78.7 ± 6.1	74.7 ± 6.2
12	22.2 ± 5.8	23.7 ± 8.1	61.2 ± 2.5
13	23.8 ± 11.4	52.3 ± 5.4	75.8 ± 2.5
14	43.9 ± 13.8	80.4 ± 0.3	83.8 ± 1.4
15	16.4 ± 4.3	45.1 ± 5.4	70.6 ± 1.2
16	17.7 ± 1.3	28.6 ± 2.8	68.0 ± 5.0

[a]Results are means ± SEM, n = 2, 3.

Compounds **1**, **2**, **9**−**11**, **13**, and **14**, showing the most intense GIRK inhibitory activities at 1 μM concentration, were subjected to further investigations. The dose−response curves of these seven compounds were determined in detailed experiments where the effect of the compounds was tested in four concentrations on five or six cells. The GIRK current was considerably reduced by these diterpenoids in a concentration-dependent manner. The effects on the inward current were statistically significant in all tested concentrations of the seven substances. Dose−response curves and IC_{50} values of the investigated compounds are shown in Figure 4.

Compounds **1** and **14** were the most effective diterpenoids, with IC_{50} values of 1.3 ± 0.2 and 1.5 ± 0.1 μM, respectively. The IC_{50} values of compounds **2** and **10** were similar (1.6 ± 0.2 and 1.7 ± 0.2 μM, respectively). The IC_{50} values of compound **11** were 2.6 ± 0.5 μM, of compound **9** 3.4 ± 0.1 μM, and for compound **13** 12.2 ± 0.5 μM. Original GIRK current curves during the application of different concentrations of the most effective compounds (compounds **1** and **14**) are shown in Figures 5A and 6A.

Compounds **1**, **2**, **9**−**11**, **13**, and **14** were also tested on the HEK-hERG cell line, and selectivity of their GIRK blocking effect was evaluated. Selectivity studies were performed in two concentrations (1 and 10 μM) on two cells. Compound **14** exerted a remarkable inhibitory effect on the hERG channel at a 10 μM concentration, while the other test compounds exhibited only minor effects (Table 4). However, these slight reductions of the current amplitudes were presumably and partly the consequence of the run-down phenomenon (slight and spontaneous decrease of the current). Original hERG current sweeps during the application of compounds **1** and **14** at 1 and 10 μM concentrations are shown in Figures 5B and 6B.

DOI: 10.1021/acs.jnatprod.8b00500
J. Nat. Prod. XXXX, XXX, XXX−XXX

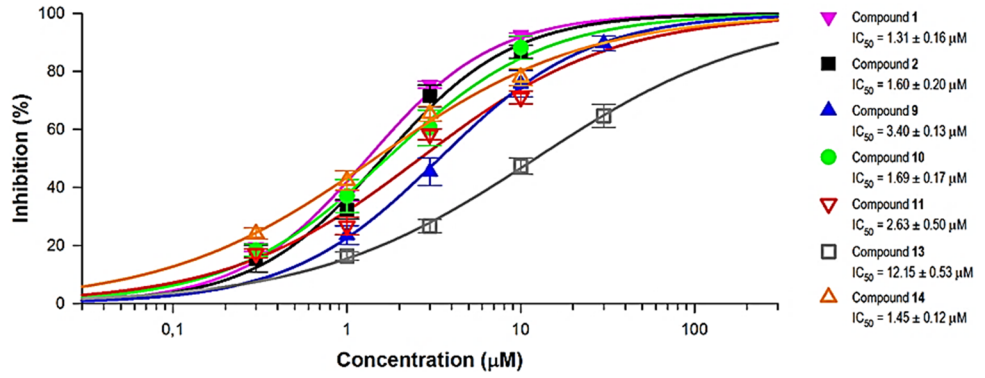

Figure 4. Dose−response curves of compounds **1**, **2**, **9**−**11**, **13**, and **14** on GIRK current. Data are expressed as means ± SEM values, n = 5, 6.

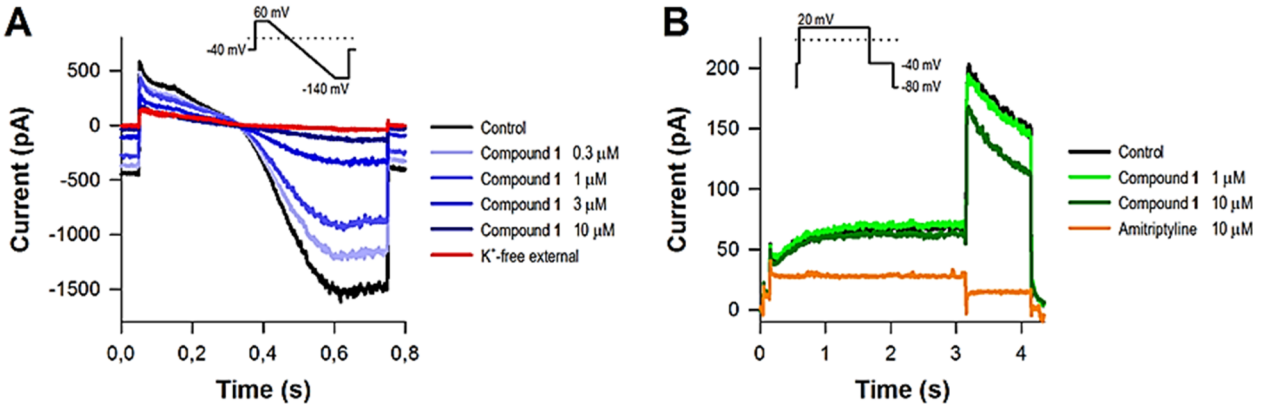

Figure 5. Effects of compound **1** on GIRK and hERG current. Panel A shows representative GIRK current curves recorded during the application of 0.3, 1, 3, and 10 μM compound **1**. The inset shows the applied GIRK voltage protocol. Application of compound **1** inhibited the GIRK current in a dose-dependent manner. The data were corrected with the current value measured in the K^+-free external solution, which served as the baseline. Panel B depicts typical hERG current sweeps during the application of 1 and 10 μM compound **1**. The inset shows the applied hERG voltage protocol. The original current traces show that compound **1** very slightly and not significantly blocked the hERG channel, while addition of reference compound amitriptyline (10 μM) fully blocked the current.

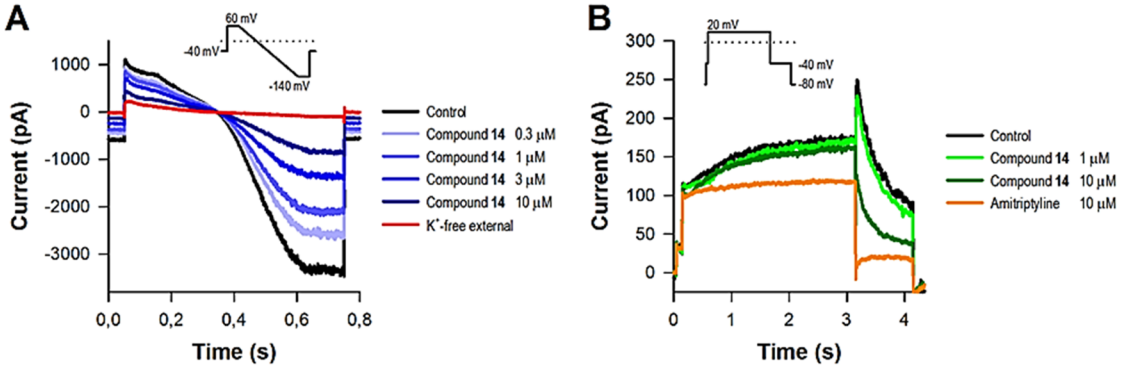

Figure 6. Concentration-dependent inhibitory effects of compound **14** on GIRK and hERG current. Panel A shows typical current curves obtained from HEK-GIRK cells treated with 0.3, 1, 3, and 10 μM compound **14**. The inset shows the applied GIRK voltage protocol. The data were corrected with the current value measured in the K^+-free external solution, which served as the baseline. Panel B shows example traces for hERG-mediated whole-cell current. Cells were treated with 1 and 10 μM compound **14**. Compound **14** very slightly and not significantly blocked the hERG channel at 1 μM concentration, while addition of 10 μM compound **14** significantly inhibited the current. The inset shows the applied hERG voltage protocol.

EXPERIMENTAL SECTION

General Experimental Procedures. The melting point of compound **1** was measured on a Linkam hot stage microscope (temperature range of −180 to 400 °C), and its thermal behavior was investigated by means of a Mettler-Toledo differential scanning calorimeter (operational range between −80 and 400 °C). Optical rotations were measured in $CHCl_3$ using a PerkinElmer 341 polarimeter. NMR spectra were recorded on a Bruker Avance DRX 500 spectrometer at 500 MHz (^{1}H) and 125 MHz (^{13}C). The residual peaks of the deuterated solvents were taken as reference points. The data were acquired and processed with MestReNova v6.0.2−5475 software. Chemical shifts are expressed in parts per million, and coupling constant (J) values are reported in Hz. High-resolution MS data were recorded on a Thermo Q Exactive Plus orbitrap mass spectrometer equipped with an ESI source and coupled with an

DOI: 10.1021/acs.jnatprod.8b00500
J. Nat. Prod. XXXX, XXX, XXX−XXX

Table 4. hERG Inhibitory Effects of Compounds 1, 2, 9−11, 13, and 14[a]

	hERG inhibition (%)		
	concentration		amitriptyline
compound	1 μM	10 μM	10 μM
1	10.8 ± 5.7	24.9 ± 6.4	97.7 ± 0.8
2	6.5 ± 5.2	24.4 ± 2.0	99.1 ± 0.9
9	11.2 ± 0.6	22.7 ± 2.6	99.3 ± 0.7
10	13.2 ± 2.2	24.0 ± 1.8	98.1 ± 0.5
11	3.3 ± 1.5	19.0 ± 0.5	99.3 ± 0.7
13	1.8 ± 0.4	7.9 ± 1.0	99.2 ± 0.8
14	11.2 ± 0.1	55.4 ± 0.4	100.0 ± 0.0

[a]Results are means ± SEM, n = 2.

Agilent 1100 HPLC system. The samples were measured with the flow injection analysis (FIA) method. The mass spectrometer was working in positive mode, and the scan mass range was set to m/z 150−2000 at a resolution of 140 000. The data were acquired and processed with Thermo Xcalibur 4.0 software. For column chromatography, polyamide (MP Polyamide, 50−160 μm, MP Biomedicals), silica gel (silica gel GF_{254}, 15 μm, Merck), and reversed-phase silica (LiChroprep RP-18, 40−63 μm, Merck) were used. HPLC was carried out on a Waters Millipore instrument with UV detection at 254 nm over normal phase (LiChrospher Si 100, 5 μm, 250 × 4 mm) and reversed-phase (LiChrosper RP-18, 5 μm, 250 × 4 mm) columns. Preparative TLC was performed on aluminum sheets coated with normal (TLC silica gel 60 F_{254}, Merck) and reversed-phase (TLC silica gel 60 RP-18 F_{254S}, Merck) silica.

Plant Material. The plant was collected at Homoródalmás, Romania, in July 2014 and was identified by one of the authors, G.J. A voucher specimen (No. 838) has been deposited in the Herbarium of the Department of Pharmacognosy, University of Szeged, Szeged, Hungary.

Extraction and Isolation. The frozen whole plant of *E. dulcis* (3800 g) was crushed in a blender and percolated with MeOH (30 L) at room temperature. The crude extract was concentrated in vacuo and exhaustively extracted with $CHCl_3$ (5 × 500 mL). The organic phase gave a residue (33.6 g), which was chromatographed on a polyamide column (160 g) with mixtures of MeOH and H_2O (3:2 and 4:1, 4.5, and 2.2 L, respectively) as eluents. The fraction obtained with MeOH−H_2O (3:2) was subjected to silica gel vacuum liquid chromatography (VLC) using a gradient solvent system of cyclohexane−EtOAc−EtOH (70:10:0, 60:10:0, 50:10:0, 50:10:1, 40:10:1, 30:10:1, and 20:10:1; each 200 mL) to yield 55 fractions (each 25 mL). The eluates were monitored by TLC. Fractions with the same chromatographic profile were combined. Pooled fraction 21−32, obtained with cyclohexane−EtOAc−EtOH (50:10:1) was further separated by reversed-phase silica gel column chromatography (A) with step gradient of mobile phase composed of MeOH−H_2O (6:4, 7:3, 8:2, 10:2, and 10:1; each 100 mL) to give 45 subfractions (A1−45, each 10 mL). Purification of A20 was carried out by means of RP-HPLC (flow rate: 1.5 mL/min, MeCN-H_2O 7:3, isocratic elution). Peaks eluted at retention times of 6.8 and 8.5 min afforded compound **11** (23.1 mg) and **2** (83.0 mg). Separation of A21−25 was performed under the same conditions and resulted in the isolation of compound **1** (t_R: 11.5 min, 177.4 mg) and an additional portion of **2** (35.3 mg). Fraction A29−36 was subjected to preparative TLC using toluene−Me_2CO (10:2) as mobile phase to yield compound **3** (9.4 mg). Fraction 38−47, eluted with cyclohexane−EtOAc−EtOH (30:10:1) was transferred to a reversed-phase silica gel column (B) using a stepwise gradient of MeOH−H_2O mixtures (5:5, 6:4, 7:3, 8:2, and 9:1; each 200 mL) to afford 62 subfractions (B1−62, each 15 mL). Fraction B32−42 was further fractionated by VLC (C) on silica gel with increasing polarity of toluene−$CHCl_3$−acetone (70:10:1, 50 mL; 60:10:1, 50 mL; 50:10:1, 50 mL; 40:10:1, 50 mL; 30:10:1, 100 mL; 20:10:1, 100 mL; 10:10:1, 50 mL) to furnish 27 eluates (C1−27, each 15 mL). Fractions C6−7 and C8−10 were chromatographed by RP-HPLC (flow rate: 1.5 mL/min, MeCN−H_2O, 6:4, isocratic elution) to give compounds **10** (8.2 mg) and **9** (8.0 mg) observed at retention times of 7.2 and 8.0 min, respectively. The final steps of purifying fraction C11−24 involved consecutive techniques of preparative TLC with the use of a cyclohexane−$CHCl_3$−MeOH (15:10:1) mobile phase and RP-HPLC (flow rate: 1.5 mL/min, MeCN−H_2O 1:1, isocratic elution). Peaks collected at retention times of 9.2, 12.5, and 17.4 min yielded pure compounds **8** (8.5 mg), **7** (16.8 mg), and **6** (22.1 mg), respectively. Compounds **4** (3.2 mg) and **5** (5.1 mg) were isolated from fraction B49−56 after repetitive purification by preparative TLC over normal- and reversed-phase silica gel employing mobile phases of toluene−acetone (4:1) and MeOH−H_2O (11:2), respectively.

*(2S,3S,4S,7R,9R,13S,14S,15R)-9α,14β-Diacetoxy-3β-benzoyloxy-15β-hydroxy-7β-tigloyloxyjatropha-5E,11E-diene (**1**):* colorless, needle-like material; mp of the minuscule needles obtained from the melt of the compound (in Supporting Information) 141.5 °C; $[\alpha]^{26}_D$ −26 (c 0.3, $CHCl_3$); for ^1H and ^{13}C NMR spectroscopic data, see Tables 1 and 2; HRESIMS m/z 625.3371 $[M + H]^+$ (calcd for $C_{36}H_{49}O_9$ 625.3377).

*8β,9α,14β-Triacetoxy-3β-benzoyloxy-15β-hydroxy-7β-tigloyloxy-jatropha-5E,11E-diene (**2**):* white, amorphous solid; $[\alpha]^{27}_D$ −196 (c 0.2, $CHCl_3$); for ^1H and ^{13}C NMR spectroscopic data, see Tables 1 and 2; HRESIMS m/z 705.3281 $[M + Na]^+$ (calcd for $C_{38}H_{50}O_{11}Na$ 705.3251), 721.3019 $[M + K]^+$ (calcd for $C_{38}H_{50}O_{11}K$ 721.2990) and 700.3731 $[M + NH_4]^+$ (calcd for $C_{38}H_{54}O_{11}N$ 700.3697).

*8β,9α-Diacetoxy-3β-benzoyloxy-15β-hydroxy-7β,14β-ditigloyloxyjatropha-5E,11E-diene (**3**):* white, amorphous powder; $[\alpha]^{27}_D$ −18 (c 0.3, $CHCl_3$); for ^1H and ^{13}C NMR spectroscopic data, see Tables 1 and 2; HRESIMS m/z 745.3596 $[M + Na]^+$ (calcd for $C_{41}H_{54}O_{11}Na$ 745.3564), 761.3333 $[M + K]^+$ (calcd for $C_{41}H_{54}O_{11}K$ 761.3303) and 740.4048 $[M + NH_4]^+$ (calcd for $C_{41}H_{58}O_{11}N$ 740.4010).

*8β,9α-Diacetoxy-3β-benzoyloxy-7β,15β-dihydroxy-14β-tigloyloxyjatropha-5E,11E-diene (**4**):* white, amorphous powder; $[\alpha]^{27}_D$ −11 (c 0.2, $CHCl_3$); for ^1H and ^{13}C NMR spectroscopic data, see Tables 1 and 2; HRESIMS m/z 663.3172 $[M + Na]^+$ (calcd for $C_{36}H_{48}O_{10}Na$ 663.3145), 679.2909 $[M + K]^+$ (calcd for $C_{36}H_{48}O_{10}K$ 679.2885) and 658.3623 $[M + NH_4]^+$ (calcd for $C_{36}H_{52}O_{10}N$ 658.3591).

*8β,9α,14β-Triacetoxy-3β-benzoyloxy-7β,15β-dihydroxyjatropha-5E,11E-diene (**5**):* white, amorphous powder; $[\alpha]^{26}_D$ −11 (c 0.2, $CHCl_3$); for ^1H and ^{13}C NMR spectroscopic data, see Tables 1 and 2; HRESIMS m/z 623.2858 $[M + Na]^+$ (calcd for $C_{33}H_{44}O_{10}Na$ 623.2832), 639.2596 $[M + K]^+$ (calcd for $C_{33}H_{44}O_{10}K$ 639.2572) and 618.3308 $[M + NH_4]^+$ (calcd for $C_{33}H_{48}O_{10}N$ 618.3278).

*7β,9α,14β-Triacetoxy-3β-benzoyloxy-8β,15β-dihydroxyjatropha-5E,11E-diene (**6**):* white, amorphous powder; $[\alpha]^{26}_D$ −10 (c 0.2, $CHCl_3$); for ^1H and ^{13}C NMR spectroscopic data, see Tables 1 and 2; HRESIMS m/z 623.2816 $[M + Na]^+$ (calcd for $C_{33}H_{44}O_{10}Na$ 623.2832), 618.3263 $[M + NH_4]^+$ (calcd for $C_{33}H_{48}O_{10}N$ 618.3278) and 583.2891 $[M - H_2O + H]^+$ (calcd for $C_{33}H_{43}O_9$ 583.2907).

*7β,14β-Diacetoxy-3β-benzoyloxy-8β,9α,15β-trihydroxyjatropha-5E,11E-diene (**7**):* white, amorphous powder; $[\alpha]^{26}_D$ −27 (c 0.2, $CHCl_3$); for ^1H and ^{13}C NMR spectroscopic data, see Tables 1 and 2; HRESIMS m/z 581.2732 $[M + Na]^+$ (calcd for $C_{31}H_{42}O_9Na$ 581.2727), 597.2466 $[M + K]^+$ (calcd for $C_{31}H_{42}O_9K$ 597.2466).

*14β-Acetoxy-3β-benzoyloxy-7β,8β,9α,15β-tetrahydroxyjatropha-5E,11E-diene (**8**):* white, amorphous powder; $[\alpha]^{26}_D$ −41 (c 0.1, $CHCl_3$); for ^1H and ^{13}C NMR spectroscopic data, see Tables 1 and 2; HRESIMS m/z 539.2644 $[M + Na]^+$ (calcd for $C_{29}H_{40}O_8Na$ 539.2621), 555.2376 $[M + K]^+$ (calcd for $C_{29}H_{40}O_8K$ 555.2360) and 534.3087 $[M + NH_4]^+$ (calcd for $C_{29}H_{44}O_8N$ 534.3067).

*7β,8β,9α,15β-Tetraacetoxy-3β-benzoyloxy-14β-hydroxyjatropha-5E,11E-diene (**9**):* white, amorphous powder; $[\alpha]^{26}_D$ +5.5 (c 0.4, $CHCl_3$); for ^1H and ^{13}C NMR spectroscopic data, see Tables 1 and 2; HRESIMS m/z 665.2960 $[M + Na]^+$ (calcd for $C_{35}H_{46}O_{11}Na$ 665.2938) and 660.3411 $[M + NH_4]^+$ (calcd for $C_{35}H_{50}O_{11}N$ 660.3384).

Automated Planar Patch-Clamp Measurements. GIRK and hERG ion currents were measured using the planar patch-clamp

DOI: 10.1021/acs.jnatprod.8b00500
J. Nat. Prod. XXXX, XXX, XXX−XXX

technology as described by Vasas et al.[16] The pipetting protocols were controlled by PatchControlHT 1.09.30 software (Nanion Technologies GmbH, Munich, Germany). Data acquisition and online analysis were performed with an EPC-10 Quadro patch-clamp amplifier (HEKA Elektronik Dr. Schulze GmbH, Lambrecht/Pfalz, Germany), using PatchMaster 2.65 software (HEKA Elektronik Dr. Schulze GmbH, Lambrecht/Pfalz, Germany). Currents were low-pass filtered at 2.9 kHz using the internal Bessel filter of the amplifier and digitized at 10 kHz.

GIRK Channel Inhibitory Assay. Experiments were carried out on HEK-293 (human embryonic kidney) cells stably expressing the GIRK1/4 (Kir3.1/3.4) K^+ channels by adapting a method described earlier.[16,27]

hERG Channel Inhibitory Assay. hERG measurements were performed on HEK-293 cells stably transfected with cDNA encoding the hERG (Kv11.1) K^+ channel as described earlier.[16,28] Increasing concentrations of the test compound (1 and 10 μM, respectively) were applied.

Statistics. All data are expressed as arithmetic means ± standard error (SEM). Statistical analysis was performed with Student's t test for paired data and corrected using the Holm−Bonferroni method. Differences were considered statistically significant when the P value was less than 0.05.

Single-Crystal Diffraction. Crystal data of **1**: $C_{36}H_{48}O_9$, fw: 1874.22, colorless needle, size: 0.15 × 0.02 × 0.02 mm, monoclinic, space group $P2_1$, a = 14.1355(4) Å, b = 18.3034(4) Å, c = 20.5777(6) Å, α = 90°, β = 97.024(3)°, γ = 90°, V = 5284.1(2) Å^3, T = 100(2) K, Z = 2, Z' = 3, $F(000)$ = 2016, D_x = 1.178 Mg/m^3, μ = 0.084 mm^{-1}. A crystal of **1** was mounted on a Kapton loop. Cell parameters were determined by least-squares using 31 964 ($1.7040° \leq \theta \leq 30.9450°$) reflections. Intensity data were collected at synchrotron SOLEIL at the PROXIMA 1 beamline (λ = 0.799 90 Å, beam size HxV = 40 × 30 μm^2) at 100(2) K in the range of $1.682° \leq \theta \leq 31.198°$. A total of 55 224 reflections were collected, of which 19 397 were unique [R(int) = 0.0477, $R(\sigma)$ = 0.0387]; intensities of 17 001 reflections were greater than $2\sigma(I)$. Completeness to θ_{max} is 0.819. A multiscan absorption correction was applied to the data (the minimum and maximum transmission factors were 0.566 83 and 1.000 00). The structure was solved by direct methods.[29] Anisotropic full-matrix least-squares refinement[29] on F^2 for all non-hydrogen atoms yielded R_1 = 0.0613 and wR_2 = 0.1714 for 1332 [$I > 2\sigma(I)$] and R_1 = 0.0659 and wR_2 = 0.1786 for all (19 397) intensity data, (number of parameters = 1249, goodness-of-fit = 1.078, the maximum and mean shift/esd is 0.167 and 0.010 for rotating terminal hydrogen of C17). The absolute structure parameter is −0.2(5)[30] (Friedel coverage: 0.910, Friedel fraction max.: 0.793, Friedel fraction full: 0.946). The maximum and minimum residual electron density in the final difference map was 0.478 and −0.310 e Å^{-3}. The weighting scheme applied was $w = 1/[\sigma^2(F_o^2) + (0.131\,600\,000P)^2 + 0.0000P]$ where $P = (F_o^2 + 2F_c^2)/3$. Hydrogen atomic positions were located in difference maps. Hydrogen atoms were included in structure factor calculations, but they were not refined. The isotropic displacement parameters of the hydrogen atoms were approximated from the U(eq) value of the atom they were bonded to.

Crystallographic data for compound **1** have been deposited with the Cambridge Crystallographic Data Centre (deposit no. 1849750). Copies of the data can be obtained, free of charge, on application to CCDC, 12 Union Road, Cambridge CB2 1EZ, UK (fax: +44-(0) 1223-336033 or e-mail: deposite@ccdc.cam.ac.uk).

■ ASSOCIATED CONTENT

Supporting Information

The Supporting Information is available free of charge on the ACS Publications website at DOI: 10.1021/acs.jnatprod.8b00500.

Copies of HRESIMS, ^{1}H, ^{13}C, ^{1}H−^{1}H COSY, HSQC, HMBC, NOESY spectra of **1**−**9**, ^{1}H NMR spectra of **10** and **11**, crystal growth, DSC curve, crystal data and details of the structure determination and refinement of compound **1**, structures of compounds **12**−**16** (PDF)

Crystallographic data for compound **1** (CIF)

■ AUTHOR INFORMATION

Corresponding Author

*Phone: +36 62 546453. Fax: +36 62 547404. E-mail: hohmann@pharm.u-szeged.hu.

ORCID

Judit Hohmann: 0000-0002-2887-6392

Dóra Rédei: 0000-0002-5013-247X

Notes

The authors declare no competing financial interest.

■ ACKNOWLEDGMENTS

The project was supported by Economic Development and Innovation Operative Programme GINOP-2.3.2-15-2016-00012 and Ministry of Human Capacities, Hungary grant 20391-3/2018/FEKUSTRAT. L.B. and P.B. are grateful for the grant of the National Research, Development and Innovation Office OTKA K124544. D.R. is a grantee of the János Bolyai Research Fellowship of the Hungarian Academy of Sciences. The authors warmly thank L. Chavas for allocating some beam time at the PROXIMA-1 beamline at synchrotron SOLEIL and T. Isabet for experimental and data processing help.

■ REFERENCES

(1) Morin, D. P.; Bernard, M. L.; Madias, C.; Rogers, P. A.; Thihalolipavan, S.; Estes, N. A. M. *Mayo Clin. Proc.* **2016**, *91*, 1778−1810.

(2) January, C. T.; Wann, L. S.; Alpert, J. S.; Calkins, H.; Cigarroa, J. E.; Cleveland, J. C., JR; Conti, J. B.; Ellinor, P. T.; Ezekowitz, M. D.; Field, M. E.; Murray, K. T.; Sacco, R. L.; Stevenson, W. G.; Tchou, P. J.; Tracy, C. M.; Yancy, C. W. *Circulation* **2014**, *130*, 2071−2104.

(3) Wolowacz, S. E.; Samuel, M.; Brennan, V. K.; Jasso-Mosqueda, J.-G.; Van Gelder, I. C. *Europace* **2011**, *13*, 1375−1385.

(4) Centers for Disease Control and Prevention, Division for Heart Disease and Stroke Prevention. Atrial Fibrillation Fact Sheet, 2017. https://www.cdc.gov/dhdsp/data_statistics/fact_sheets/fs_atrial_fibrillation.htm (accessed May 12, 2018).

(5) Woods, C. E.; Olgin, J. *Circ. Res.* **2014**, *114*, 1532−1546.

(6) Chen, P.-S.; Chen, L. S.; Fishbein, M. C.; Lin, S.-F.; Nattel, S. *Circ. Res.* **2014**, *114*, 1500−1515.

(7) Walsh, K. B. *Front. Pharmacol.* **2011**, *2*, Article 64, 1−8 .

(8) Hashimoto, N.; Yamashita, T.; Tsuruzoe, N. *Pharmacol. Res.* **2006**, *54*, 136−141.

(9) Vandenberg, J. I.; Perry, M. D.; Perrin, M. J.; Mann, S. A.; Ke, Y.; Hill, A. P. *Physiol. Rev.* **2012**, *92*, 1393−1478.

(10) Sanguinetti, M. C.; Tristani-Firouzi, M. *Nature* **2006**, *440*, 463−469.

(11) De Bruin, M. L.; Pettersson, M.; Meyboom, R. H. B.; Hoes, A. W.; Leufkens, H. G. M. *Eur. Heart J.* **2005**, *26*, 590−597.

(12) Whitebread, S.; Hamon, J.; Bojanic, D.; Urban, L. *Drug Discovery Today* **2005**, *10*, 1421−1433.

(13) Rédei, D.; Forgo, P.; Molnár, J.; Szabó, P.; Zorig, T.; Hohmann, J. *Tetrahedron* **2012**, *68*, 8403−8407.

(14) Islam, M. T. *Phytother. Res.* **2017**, *31*, 691−712.

(15) Nothias-Scaglia, L.-F.; Retailleau, P.; Paolini, J.; Pannecouque, C.; Neyts, J.; Dumontet, V.; Roussi, F.; Leyssen, P.; Costa, J.; Litaudon, M. *J. Nat. Prod.* **2014**, *77*, 1505−1512.

(16) Vasas, A.; Forgó, P.; Orvos, P.; Tálosi, L.; Csorba, A.; Pinke, Gy.; Hohmann, J. *J. Nat. Prod.* **2016**, *79*, 1990−2004.

(17) De Mieri, M.; Du, K.; Neuburger, M.; Saxena, P.; Zietsman, P. C.; Hering, S.; van der Westhuizen, J. H.; Hamburger, M. *J. Nat. Prod.* **2015**, *78*, 1697−1707.

DOI: 10.1021/acs.jnatprod.8b00500
J. Nat. Prod. XXXX, XXX, XXX−XXX

(18) Kúsz, N.; Orvos, P.; Csorba, A.; Tálosi, L.; Chaieb, M.; Hohmann, J.; Rédei, D. *Tetrahedron* **2016**, *72*, 5724−5728.
(19) Pohl, R.; Janistyn, B.; Nahrstedt, A. *Planta Med.* **1975**, *27*, 301−303.
(20) Rédei, D.; Kúsz, N.; Sátori, G.; Kincses, A.; Spengler, G.; Burián, K.; Barina, Z.; Hohmann, J. *Planta Med.* **2018**, *84*, 729−735.
(21) Marco, J. A.; Sanz-Cervera, J. F.; Yuste, A.; Jakupovic, J.; Jeske, F. *Phytochemistry* **1998**, *47*, 1621−1630.
(22) Valente, I.; Reis, M.; Duarte, N.; Serly, J.; Molnár, J.; Ferreira, M.-J. U. *J. Nat. Prod.* **2012**, *75*, 1915−1921.
(23) Esposito, M.; Nothias, L.-F.; Nedev, H.; Gallard, J.-F.; Leyssen, P.; Retailleau, P.; Costa, J.; Roussi, F.; Iorga, B. I.; Paolini, J.; Litaudon, M. *J. Nat. Prod.* **2016**, *79*, 2873−2882.
(24) Barile, E.; Borriello, M.; Di Pietro, A.; Doreau, A.; Fattorusso, C.; Fattorusso, E.; Lanzotti, V. *Org. Biomol. Chem.* **2008**, *6*, 1756−1762.
(25) Nothias-Scaglia, L.-F.; Gallard, J.-F.; Dumontet, V.; Roussi, F.; Costa, J.; Iorga, B. I.; Paolini, J.; Litaudon, M. *J. Nat. Prod.* **2015**, *78*, 2423−2431.
(26) Yamamura, S.; Shizuri, Y.; Kosemura, S.; Ohtsuka, J.; Tayama, T.; Ohba, S.; Ito, M.; Saito, Y.; Terada, Y. *Phytochemistry* **1989**, *28*, 3421−3436.
(27) Nanion technologies - Products - Patchliner, https://www.nanion.de/en/products/patchliner.html (accessed May 29, 2018).
(28) Orvos, P.; Virág, L.; Tálosi, L.; Hajdú, Zs.; Csupor, D.; Jedlinszki, N.; Szél, T.; Varró, A.; Hohmann, J. *Fitoterapia* **2015**, *100*, 156−165.
(29) Sheldrick, G. M. *Acta Crystallogr., Sect. A: Found. Crystallogr.* **2008**, *64*, 112−122.
(30) Flack, H. D. *Acta Crystallogr., Sect. A: Found. Crystallogr.* **1983**, *39*, 876−881.

DOI: 10.1021/acs.jnatprod.8b00500
J. Nat. Prod. XXXX, XXX, XXX−XXX